Adaptive Time-Stepping Universal Line and Machine Models for Real Time and Faster-Than-Real-Time Hardware Emulation

Tong Duan, *Student Member, IEEE*, and Venkata Dinavahi, *Senior Member, IEEE*

***Abstract*—Transmission lines and rotating machines that widely exist in power systems should be accurately modeled in real-time electromagnetic transient (EMT) simulation for obtaining precise results for hardware-in-the-loop applications. In the conventional EMT simulator, the time-step is fixed, which may lead to inefficiencies when the time constants of the system change. The adaptive time-stepping (ATS) method can efficaciously solve this problem; however, the ATS schemes for the universal transmission line model (ULM) and universal machine (UM) model remain to be investigated. This article derives the ATS models for ULM and UM, and the proposed ULM model is more stable than the traditional model. Both ATS models are emulated on the parallel and pipelined architecture of the field-programmable gate array (FPGA). The proposed subsystem-based ATS scheme and the local truncation error (LTE) based time-step control enable the large-scale systems to be simulated in real time and "faster-than-real-time" modes. The IEEE 39-bus system with ATS models is emulated on two interconnected FPGA boards, and the emulation results compared with PSCAD/EMTDC and fixed time-stepping (FTS) hardware emulator verify the effectiveness of the proposed models and show that the LTE of ULM and UM can be reduced by 76.5% and 62.0%, respectively, compared with the FTS simulation.**

***Index Terms*—Adaptive time-step (ATS), electromagnetic transients (EMTs), faster-than-real-time, field-programmable gate arrays (FPGA), hardware emulation, parallel processing, real-time systems, universal machine (UM), universal transmission line.**

I. Introduction

REAL-TIME electromagnetic transient (EMT) simulation is a paramount tool to reproduce the power system behavior over transients such as switching overvoltages and lightning surges before the tested controller or protective device is deployed in the real world [1]–[4]. Most real-time simulators as well as offline EMT simulators such as the PSCAD/EMTDC [5] and EMTP-RV use a fixed time-step (FTS) to proceed the simulation; however, it may be not an efficient approach when the time constants of a system are widely varying and do not change very frequently. For example, a large time-step is usually enough to show the waveforms under normal steady-state conditions, but a small time-step is required when the fast transients happen. To accelerate the simulation process without losing accuracy, the variable time-stepping method that changes the time-step during simulation according to accuracy requirements has been studied and applied in power system simulation [6]–[13].

Transmission lines and synchronous generators are crucial components of power systems and their accurate modeling has a significant impact on real-time EMT simulation results. The line model can be divided into the constant parameter traveling-wave line model and frequency-dependent line model (FDLM) [14]. The traveling-wave line model uses constant line parameters (R, L, C, G); however, the line parameters in reality are not fixed but are functions of frequency, which influence the line behavior over a wide transient range. The universal line model (ULM) [15] is a phase-domain FDLM, which is considered to be efficient and robust for both overhead lines and underground cables. Although rotating electric machines can be categorized into many different types, such as the synchronous machine and induction machine that may have different machine-to-network interfaces or mechanical systems, their electrical equations can be unified into the same form, which led to the universal machine (UM) model [16].

Since the ULM and UM model serve a wide range of transmission lines and rotating machines, they are required to be properly modeled for adaptive time-stepping (ATS) EMT simulation. Although the variable time-stepping model for the traveling-wave line model has already been studied in [7] and [9], to the best of our knowledge, the ATS models for ULM and UM have not been derived. Ramirez and Iravani [10], Camara *et al.* [11] applied the variable time-stepping simulation in frequency domain, but the frequency-domain line model was simplified without involving the convolution process and both simulated the system in software but not in hardware for real time. Shen and Dinavahi [12] implemented the variable time-stepping simulation in real time

Manuscript received May 3, 2019; revised June 26, 2019; accepted August 5, 2019. Date of publication August 28, 2019; date of current version March 31, 2020. This work was supported in part by the Natural Science and Engineering Research Council of Canada and in part by China Scholarship Council. *(Corresponding author: Tong Duan.)*

The authors are with the Department of Electrical and Computer Engineering, University of Alberta, Edmonton, AB T6G 2V4, Canada (e-mail: tduan@ualberta.ca; dinavahi@ualberta.ca).

Color versions of one or more of the figures in this article are available online at http://ieeexplore.ieee.org.

Digital Object Identifier 10.1109/TIE.2019.2935930

with nonlinear systems such as the power electronic converter and surge arresters, however, the time-steps are the same with all equipment, which is not suitable for the ATS simulation of large-scale systems. Although the system decomposition can be applied to use different time-steps for different subsystems [17], the time-step of each subsystem also changes in the ATS simulation; thus how to deal with data exchange and synchronization between subsystems with variable time-steps remains to be discussed.

Based on this observation, this article first derives the ATS model for universal transmission lines and UMs, and then the proposed models are emulated in both real time and "*faster-than-real-time*" (FTRT) on the field-programmable gate array (FPGA) with large-scale test systems. Different with the work [12] that uses dV/dt or dI/dt as the time-step changing criteria, the time-step control in this article is based on the local truncation error (LTE). Since the dV/dt value will also change as a sin function in a steady-state sinusoidal waveform, there will be a big difference in dV/dt value change when the transient happens at the different places of a waveform, which may not be accurate enough to show the system perturbation. By applying the subsystem-based ATS simulation architecture, the simulation process can be accelerated to achieve a FTRT simulation. The main contributions of the proposed ATS modeling and hardware emulator are the following:

1) The proposed *process-reversed* ULM model significantly improves the stability when the time-step changes compared with the traditional ULM model.
2) The step-size control is based on LTE and is independent between various subsystems to achieve high accuracy when simulating large-scale power systems.
3) FTRT execution is achieved in hardware by proper coordination between subsystems with different variable time-steps.

The simulation results of the IEEE 39-bus test system are compared with PSCAD/EMTDC and the developed fixed time-stepping hardware emulator to verify the efficacy of the proposed models and the acceleration through the ATS method. The rest of this article is organized as follows. Section II introduces the proposed subsystem-based ATS method and time-step control schemes. Section III derives the ATS models for the ULM and UM. Section IV introduces the FPGA-based hardware platform and emulation of the case study. Section V presents the emulation results and the validation. Section VI concludes this article.

II. ATS for the EMT Simulation

The ATS process is determined by the properly selected discretization method and time-step control scheme, and based on which the specific equipment models are involved in the EMT simulation.

A. One-Step Method

Typically, a power system containing linear or nonlinear dynamic elements can be formulated as a series of differential equations expressed as: $\boldsymbol{x} = f(\boldsymbol{x}, t)$. The practical approach for solving these differential equations is to repeatedly discretize them and solve the resulting algebraic equations. The uniform discretization method is the linear multistep (LMS) method

$$\sum_{j=0}^{k} \alpha_j \boldsymbol{x}_{n-j} = \Delta t \sum_{j=0}^{k} \beta_j \boldsymbol{f}_{n-j} \tag{1}$$

where k is the step-number and if $k = 1$, it is called one-step method. If $\beta_0 = 0$, the method is explicit, otherwise it is implicit.

The time-step Δt in (1) is assumed to be fixed. As for the ATS method in which the time-step Δt may change, the LMS method requires to be rederived for the case of nonequidistant data. But one-step methods require no modification to their formulas, that is,

$$\sum_{j=0}^{1} \alpha_j \boldsymbol{x}_{n-j} = \Delta t_n \sum_{j=0}^{1} \beta_j \boldsymbol{f}_{n-j} \tag{2}$$

$$\Delta t_n = t_n - t_{n-1}. \tag{3}$$

Higher order formulas are useful because they can be more accurate, however, it becomes more complicated to derive the LMS method with an adaptive time-step. Since the commonly used discretization methods such as the forward Euler, backward Euler (BE), and trapezoidal rule (TR) method are all one-step methods, they are the main focus of this article.

B. Adaptive Time-Step Control

Among these three one-step LMS methods, BE and TR are both convergent and zero-stable, which means the time-step control can be based solely on the consideration of accuracy without considering the convergence and stability [18]. Therefore, in this article, the TR method is applied for all the system equipment and the time-step control is based on the consideration of accuracy, which is always represented by the LTE defined as follows:

$$\mathrm{LTE}(t_n) = \boldsymbol{x}(t_n) - \tilde{\boldsymbol{x}}_n \approx C_{p+1} \Delta t_n^{p+1} \boldsymbol{x}^{(p+1)}(t_{n-1}) \tag{4}$$

where $\boldsymbol{x}(t_n)$ is the exact solution at t_n, and $\boldsymbol{x}_n$ is the solution returned by the k-step LMS method when artificially setting $\boldsymbol{x}_{n-j} = \boldsymbol{x}(t_{n-j})$ for $j = 0, 1, \ldots, k-1$. C_{p+1} is the error constant of a specific LMS method; $\boldsymbol{x}^{(p+1)}(t_{n-1})$ means the $(p+1)$th derivative of $\boldsymbol{x}$ evaluated at t_{n-1}, which is usually difficult to find. Thus, alternative approaches are applied to estimate the LTE

$$\mathrm{LTE}(t_n) \approx C_{p+1} \Delta t_n^{p+1} (p+1)! \, \boldsymbol{g}[t_n, \ldots, t_{n-1-p}] \tag{5}$$

where $\boldsymbol{g}[t_n, \ldots, t_{n-k}]$ can be calculated step-by-step: $\boldsymbol{g}(t_n) = \boldsymbol{x}_n$ and

$$\boldsymbol{g}[t_n, \ldots, t_{n-k}] = \frac{\boldsymbol{g}[t_n, \ldots, t_{n-k+1}] - \boldsymbol{g}[t_{n-1}, \ldots, t_{n-k}]}{t_n - t_{n-k}}. \tag{6}$$

Once the LTE at t_n is obtained, the next time-step is supposed to change to

$$\Delta t_{n+1} \approx \Delta t_n \min \left| \frac{\epsilon(i)}{\epsilon_n(i)} \right|^{\frac{1}{p+1}} \tag{7}$$

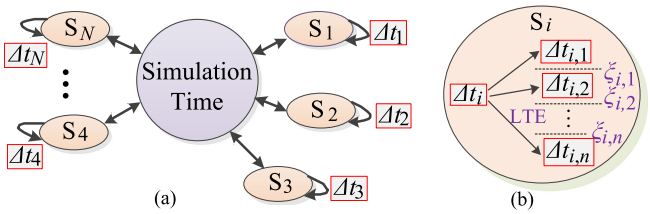

Fig. 1. Subsystem-based ATS scheme. (a) Global scheme. (b) Local subsystem scheme.

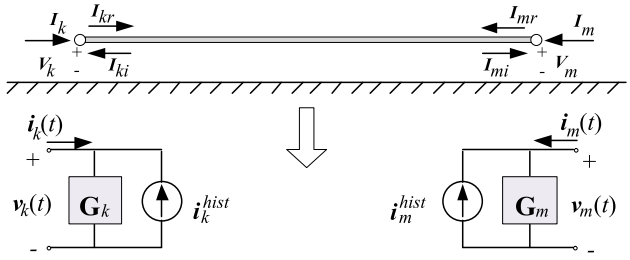

Fig. 2. Equivalent circuit of the ULM.

where $\epsilon_n = \text{LTE}(t_n)$ is computed and ϵ is the desired LTE at t_{n+1}.

C. Proposed Subsystem-Based ATS Scheme

Since in this article the system is simulated in hardware and all the parameters related to the time-steps are stored in advance, it is infeasible to change the time-step arbitrarily. Thus in general, there should be several predetermined candidate time-steps, and the time-step adaption is determined by the LTE of the previous step and the threshold. Considering that the state-variables and time-constants of different equipment (such as ULMs, UMs, and transformers) are also different, this article proposes a subsystem-based ATS scheme, as shown in Fig. 1. Each subsystem ($S_i, 1 \leqslant i \leqslant N$) holds its own time-step set $\{\Delta t_{i,1}, \Delta t_{i,2}, \ldots, \Delta t_{i,n_i}\}$ and LTE threshold $\{\xi_{i,1}, \xi_{i,2}, \ldots, \xi_{i,n_i}\}$, and changes the time-step Δt_i locally while synchronizing to the simulation time of the whole system. Note that since the LTE threshold of various components within a subsystem are also different, the time-step of a subsystem will change if any components exceed their own LTE threshold.

Although the whole system can be divided into subsystems and each subsystem can run in different time-steps, their time-step size also cannot be arbitrarily assigned due to the necessity of synchronization. For example, if a subsystem uses a 10 μs time-step and the connected subsystem uses a 13 μs time-step, then it will be extremely complicated to synchronize the two subsystems because they could not reach at the same synchronization point after each time-step. Therefore, in this article, the time-step sizes of different subsystems are always linearly proportional to each other. Then all subsystems can proceed to the same synchronization point with different time-steps, and the time-space to the next synchronization point is the maximum time-step of these subsystems. Since their time-steps are all linearly proportional, the other subsystems with smaller time-steps are only required to execute several times to reach that synchronization point. Therefore, the adaptive multiple variable time-stepping method will be executed as follows:

1) Calculate the LTE of different equipment at t_{n-1}.
2) Increase or decrease the time-step locally based on the specific threshold.
3) Implement the time-step change and calculation, by accordingly updating the numerical parameters.
4) Synchronize the results between interconnected subsystems.

III. ATS ULM and UM Models

Although TR is one-step method, the ULM and UM model computation for ATS is not the same as that for the FTS because the model parameters may change when the time-step changes.

A. Universal Transmission Line Model Computation

The equivalent circuit for ULM is shown in Fig. 2, in which the two ends (k and m) of the line are abstracted into two disconnected parts, and each part combines an equivalent conductance matrix in parallel with a compensating current source ($\boldsymbol{i}_k^{\text{hist}}$ and $\boldsymbol{i}_m^{\text{hist}}$) through which the two ends are interacting.

The electromagnetic behavior of a transmission line in frequency domain can be characterized by two matrix transfer functions: $\mathbf{Y}_c(\omega)$ the characteristic admittance matrix and $\mathbf{H}(\omega)$ the propagation matrix. The time-domain relationship between currents and voltages at the two ends can be expressed using these two matrices [15], [20]:

$$\boldsymbol{i}_k^{\text{hist}} = \mathbf{G}_k \boldsymbol{v}_k(t) - [\mathbf{y}_c * \boldsymbol{v}_k(t) - 2\mathbf{h} * \boldsymbol{i}_{mr}(t)] \tag{8}$$

$$\boldsymbol{i}_m^{\text{hist}} = \mathbf{G}_m \boldsymbol{v}_m(t) - [\mathbf{y}_c * \boldsymbol{v}_m(t) - 2\mathbf{h} * \boldsymbol{i}_{kr}(t)] \tag{9}$$

where $\mathbf{y}_c$ and $\mathbf{h}$ are obtained via an inverse Fourier transform for $\mathbf{Y}_c(\omega)$ and $\mathbf{H}(\omega)$, $\boldsymbol{i}_{kr}$ and $\boldsymbol{i}_{ki}$ are the incoming current wave and reflected current wave at k point, respectively. In practice, the convolution operation represented by the symbol "$*$" is usually not easy to carry out because $\mathbf{Y}_c(\omega)$ and $\mathbf{H}(\omega)$ may be too complex to have a simple formula in time domain. By applying proper fitting techniques [19], the time-domain elements of $\mathbf{Y}_c$ and $\mathbf{H}$ can be simplified as

$$\mathbf{y}_c^{(i,j)}(t) = \sum_{k=1}^{N_p} \mathbf{r}_{Y_c}^{(i,j,k)} e^{\mathbf{p}_{Y_c}^{(k)} t} + \mathbf{d}^{(i,j)} \delta(t) \tag{10}$$

$$\mathbf{h}^{(i,j)}(t) = \sum_{k=1}^{N_m} \sum_{n=1}^{N_{p,k}} \mathbf{r}_H^{(i,j,k,n)} e^{\mathbf{p}_H^{(k,n)}(t-\tau_k)} \tag{11}$$

where $N_p, N_{p,k}$ are the number of poles, N_m is the number of modes, and the superscript of each symbol indicates the elements of a vector or matrix. Note that the italic symbols represent vectors and nonitalic symbols denote matrices. The residue matrix $\mathbf{r}$ is a three-dimensional (3-D) matrix (for $\mathbf{Y}_c$), because it contains a 3 $\times$ 3 matrix (three conductors for example) for each pole. The pole parameter $\boldsymbol{p}$ is a vector for $\mathbf{Y}_c$ but is a matrix for $\mathbf{H}$ because it has multiple modes. $\mathbf{d}$ is the proportional terms and τ_k is the time delay for the kth mode.

In the EMT simulation, $\boldsymbol{g}(t) = \mathbf{y}_c * \boldsymbol{v}_k(t)$ convolution calculation can be discretized to be performed step-by-step by using a state variable $\boldsymbol{x} = [\boldsymbol{x}^{(1)}, \boldsymbol{x}^{(2)}, \ldots, \boldsymbol{x}^{(N_p)}]$ defined below [20]:

$$\boldsymbol{x}^{(i)}(t) = \boldsymbol{p}_{Y_c}^{(i)} \boldsymbol{x}^{(i)}(t) + \boldsymbol{v}_k(t), 1 \leqslant i \leqslant N_p \tag{12}$$

$$\boldsymbol{g}(t) = \sum_{i=1}^{N_p} \mathbf{r}_{Y_c}^{(:,:,i)} \boldsymbol{x}^{(i)}(t) + \mathbf{d}\boldsymbol{v}_k(t) \tag{13}$$

where the superscript $(:,:,i)$ means the ith 3×3 matrix of $\mathbf{r}_{Y_c}$. By applying the TR discretization, (12) could be calculated as

$$\boldsymbol{x}^{(i)}(n) = \boldsymbol{\alpha}_{Y_c}^{(i)}(n)\boldsymbol{x}^{(i)}(n-1) + \boldsymbol{\lambda}_{Y_c}^{(i)}(n)\boldsymbol{v}_k(n) + \boldsymbol{\mu}_{Y_c}^{(i)}(n)\boldsymbol{v}_k(n-1) \tag{14}$$

$$\boldsymbol{g}(n) = \sum_{i=1}^{N_p} \mathbf{r}_{Y_c}^{(:,:,i)} \boldsymbol{x}^{(i)}(n) + \mathbf{d}\boldsymbol{v}_k(n) \tag{15}$$

where

$$\boldsymbol{\alpha}_{Y_c}^{(i)}(n) = \left(1 + \boldsymbol{p}_{Y_c}^{(i)} \frac{\Delta t_n}{2}\right) \Big/ \left(1 - \boldsymbol{p}_{Y_c}^{(i)} \frac{\Delta t_n}{2}\right) \tag{16}$$

$$\boldsymbol{\lambda}_{Y_c}^{(i)}(n) = \boldsymbol{\mu}_{Y_c}^{(i)}(n) = \left(\frac{\Delta t_n}{2}\right) \Big/ \left(1 - \boldsymbol{p}_{Y_c}^{(i)} \frac{\Delta t_n}{2}\right). \tag{17}$$

Traditional Model: The traditional method [20] that is widely used in fixed time-stepping ULM model is to use a new state variable $\boldsymbol{x}^{*(i)}(n) = \boldsymbol{x}^{(i)}(n) - \boldsymbol{\lambda}_{Y_c}^{(i)}(n)\boldsymbol{v}_k(n), 1 \leqslant i \leqslant N_p$ instead to eliminate the $\boldsymbol{v}_k(n)$ item

$$\boldsymbol{x}^{*(i)}(n) = \boldsymbol{\alpha}_{Y_c}^{(i)}(n)\boldsymbol{x}^{*(i)}(n-1) + \left(\boldsymbol{\alpha}_{Y_c}^{(i)}(n)\boldsymbol{\lambda}_{Y_c}^{(i)}(n-1)\,\boldsymbol{\mu}_{Y_c}^{(i)}(n)\right)\boldsymbol{v}_k(n-1) \tag{18}$$

$$\boldsymbol{g}(n) = \sum_{i=1}^{N_p} \mathbf{r}_{Y_c}^{(:,:,i)} \boldsymbol{x}^{*(i)}(n) + \mathbf{G}_k(n)\boldsymbol{v}_k(n) \tag{19}$$

and $\mathbf{G}_k(n)$ is the equivalent conductance matrix

$$\mathbf{G}_k(n) = \mathbf{G}_m(n) = \mathbf{d} + \sum_{k=1}^{N_p} \boldsymbol{\lambda}_{Y_c}^{(k)}(n)\mathbf{r}_{Y_c}^{(:,:,k)}. \tag{20}$$

Note that $\mathbf{G}(n)\boldsymbol{v}_k(n)$ in (19) can be eliminated by the current items in (8) when calculating the equivalent current source $\boldsymbol{i}_k^{\text{hist}}$; thus $\boldsymbol{v}_k(n)$ is not required, which makes the equivalent current source to be computed only depending on the results of previous steps. The $\mathbf{h} * \boldsymbol{i}_{mr}(t)$ convolution has the same computation flow, but only the history items $\boldsymbol{i}_{mr}(t - \tau_k), k = 1, \ldots, N_m$ are needed for the calculation at time t because there is a time-delay τ_k in the $\mathbf{h}$ matrix function.

However, this traditional method for FTS may not be applicable for adaptive time-step. Because when the time-step changes, the constant $\boldsymbol{\lambda}_{Y_c}$ will change to a new value, which makes the state variable $\boldsymbol{x}^*$ actually change to a different new state variable from the one before time-step changes. That means, the new state-variable may need several steps to make itself stable and consistent with the former state-variable, which will cause instability when the time-step changes. This phenomenon will be verified later in the simulation section.

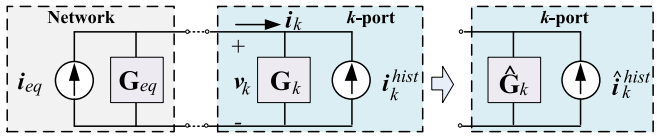

Fig. 3. Illustration for the process-reversed model for the ULM.

Process-Reversed Model: To solve the instability problem of the traditional method, this article proposes a novel current-source-based method that has a reverse logic of the traditional method. The rest of the system in each end of the transmission line can be equivalenced to a current source $\boldsymbol{i}_{eq}$ in parallel with a conductance $\mathbf{G}_{eq}$, as shown in Fig. 3. At the port k, the system equation can be written as

$$[\mathbf{G}_{eq} + \mathbf{G}_k]\boldsymbol{v}_k(t) = \boldsymbol{i}_{eq}(t) + \boldsymbol{i}_k^{\text{hist}}. \tag{21}$$

Substituting $\boldsymbol{i}_k^{\text{hist}}$ by (8) and expressing as discrete-time

$$[\mathbf{G}_{eq} + \mathbf{G}_k]\boldsymbol{v}_k(n) = \boldsymbol{i}_{eq}(n) + \mathbf{G}_k\boldsymbol{v}_k(n) - [\mathbf{y}_c * \boldsymbol{v}_k(n) - 2\mathbf{h} * \boldsymbol{i}_{mr}]. \tag{22}$$

From (14) and (15), we know

$$\mathbf{y}_c * \boldsymbol{v}_k(n) = \sum_{i=1}^{N_p} \mathbf{r}_{Y_c}^{(:,:,i)} \boldsymbol{x}^{(i)}(n) + \mathbf{d}\boldsymbol{v}_k(n). \tag{23}$$

Here, $\mathbf{G}_k(n) = \mathbf{d}$. Combining (14), (22), (23) together, we obtain

$$[\mathbf{G}_{eq} + \mathbf{G}_k + \mathbf{G}_r]\boldsymbol{v}_k(n) = \boldsymbol{i}_{eq}(n) + 2\mathbf{h} * \boldsymbol{i}_{mr} - \boldsymbol{x}^{\text{hist}} \tag{24}$$

where

$$\mathbf{G}_r = \sum_{k=1}^{N_p} \boldsymbol{\lambda}_{Y_c}^{(k)}(n)\mathbf{r}_{Y_c}^{(:,:,k)} \tag{25}$$

$$\boldsymbol{x}^{\text{hist}} = \sum_{i=1}^{N_p} \mathbf{r}_{Y_c}^{(:,:,i)} [\boldsymbol{\alpha}_{Y_c}^{(i)}(n)\boldsymbol{x}^{(i)}(n-1) + \boldsymbol{\mu}_{Y_c}^{(i)}(n)\boldsymbol{v}_k(n-1)]. \tag{26}$$

Since the convolution $\mathbf{h} * \boldsymbol{i}_{mr}$ at time t_n actually only needs the history items $\boldsymbol{i}_{mr}(t_n - \tau_k), k = 1, \ldots, N_m$, the only unknown variable to be solved at t_n in (24) is the node voltage $\boldsymbol{v}_k(n)$. Equations (24) and (26) actually generate a new equivalent admittance matrix $\hat{\mathbf{G}}_k$ and $\hat{\boldsymbol{i}}_k^{\text{hist}}$, as shown in Fig. 3, where

$$\hat{\mathbf{G}}_k = \mathbf{G}_k + \mathbf{G}_r, \quad \hat{\boldsymbol{i}}_k^{\text{hist}} = 2\mathbf{h} * \boldsymbol{i}_{mr} - \boldsymbol{x}^{\text{hist}}. \tag{27}$$

And the $\hat{\mathbf{G}}_k$ will change if the time-step changes. After the node voltages are solved, the other variables ($\boldsymbol{x}, \boldsymbol{i}_{kr}(n), \boldsymbol{i}_{mr}(n)$, etc.) at t_n can be solved based on the node voltages.

The logic of this method is totally different from the traditional method. In the traditional method, the state variables $\boldsymbol{x}^{(i)}(n)$ are calculated first to obtain $\boldsymbol{i}_k^{\text{hist}}$, and then the node voltages are solved; however, this method will cause instability when the time-step changes. In the process-reversed method, the calculation sequence is reversed: first, the node voltages are solved and then the state variables $\boldsymbol{x}(n)$ are updated. In the

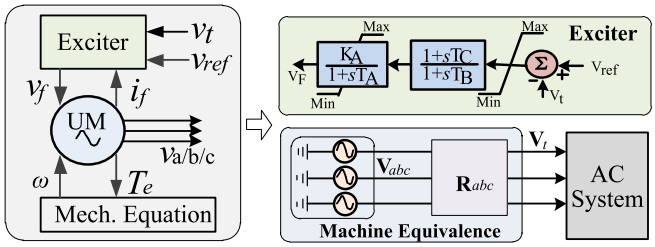

Fig. 4. Equivalent circuit for the UM model.

fixed time-stepping simulation, these two methods essentially have the same presentation, however, in the ATS simulation, using the process-reversed method the state variables $\boldsymbol{x}(n)$ will remain the same no matter how the time-step changes, which greatly improves the stability.

B. UM Model Computation

For the UM model, there are three stator windings $\{d, q, 0\}$, several damper windings $\{kd, kq\}$ in the direct and quadrature (d and q) rotor axis, and one filed windings $\{f\}$. In this article, the machine with one kd winding and two kq windings is considered as a general model to represent the synchronous generators. The fixed time-stepping model and hardware implementation can be found in [21], in which the relationship between voltages and currents can be expressed as follows:

$$\boldsymbol{v}_{um}(t) = -\mathbf{R}_{um}\boldsymbol{i}_{um}(t) - \frac{d}{dt}\boldsymbol{\psi}_{um}(t) + \boldsymbol{u}(t) \tag{28}$$

$$\boldsymbol{\psi}_{um}(t) = \mathbf{L}_{um} \cdot \boldsymbol{i}_{um}(t) \tag{29}$$

where $\boldsymbol{v}_{um} = [v_d,\ v_q,\ v_0,\ v_f,\ 0,\ 0,\ 0]^{\mathrm{T}}$, $\boldsymbol{i}_{um} = [i_d,\ i_q,\ i_0,\ i_f,\ i_{kd},\ i_{kq1},\ i_{kq2}]^{\mathrm{T}}$, $\boldsymbol{\psi}_{um} = [\psi_d,\ \psi_q,\ \psi_0,\ \psi_f,\ \psi_{kd},\ \psi_{kq1},\ \psi_{kq2}]^{\mathrm{T}}$, $\boldsymbol{u} = [-\omega\psi_q,\ \omega\psi_d,\ 0,\ 0,\ 0,\ 0,\ 0]^{\mathrm{T}}$, $\mathbf{R}_{um} = \mathrm{diag}\,(R_d, R_q, R_0, R_f, R_{kd}, R_{kq1}, R_{kq2})$ and $\mathbf{L}_{um}$ is the leakage inductance matrix.

To solve the machine equations above in discrete time, (28) is discretized using TR, which leads to a Thévenin voltage source representation [22] shown in Fig 4:

$$\boldsymbol{v}_{um}(n) = -\left[\mathbf{R}_{um} + \frac{2}{\Delta t_n}\mathbf{L_{um}} - \omega\mathbf{L_u}\right]\boldsymbol{i}_{um}(n) + \boldsymbol{v}^{\mathrm{hist}} \tag{30}$$

where

$$\boldsymbol{v}^{\mathrm{hist}} = \boldsymbol{u}(n-1) - \boldsymbol{v}_{um}(n-1) - \left[\mathbf{R}_{um} - \frac{2}{\Delta t_n}\mathbf{L}_{um}\right]\boldsymbol{i}_{um}(n-1) \tag{31}$$

and $\boldsymbol{u}(n) = \omega\mathbf{L_u}\boldsymbol{i}_{um}(n)$, $\mathbf{L_u} = [-\mathbf{L_{um}}(2); \mathbf{L_{um}}(1); \mathbf{0}; \mathbf{0}; \mathbf{0}; \mathbf{0}; \mathbf{0}]$. Note that the time-step Δt_n is not a constant but may change during the simulation process, which is different from the FTS model.

Let $\mathbf{R}_{um,eq} = [\mathbf{R}_{um} + \frac{2}{\Delta t}\mathbf{L_{um}} - \omega\mathbf{L_u}]$, and $\mathbf{R}_{um,eq} = [\mathbf{R}_{ss}\ \mathbf{R}_{sr}; \mathbf{R}_{rs}\ \mathbf{R}_{rr}]$. Then, the dq0 frame can be extracted from the vector of (30)

$$\boldsymbol{v}_{dq0}(n) = -\mathbf{R}_{ss}\boldsymbol{i}_{dq0}(n) - \mathbf{R}_{sr}\boldsymbol{i}_r(n) + \boldsymbol{v}^{\mathrm{hist}}_{dq0} \tag{32}$$

$$\boldsymbol{v}_r(n) = -\mathbf{R}_{rs}\boldsymbol{i}_{dq0}(n) - \mathbf{R}_{rr}\boldsymbol{i}_r(n) + \boldsymbol{v}^{\mathrm{hist}}_r \tag{33}$$

where $\boldsymbol{i}_r = [i_f, i_{kd}, i_{kq1}, i_{kq2}]^T$, and $\boldsymbol{v}_r = [v_f, 0, 0, 0]^T$ only contains the field voltage of which the value at time t_n is known from the exciter module. Thus from (32) and (33), the relationship between $\boldsymbol{v}_{dq0}(n)$ and $\boldsymbol{i}_{dq0}(n)$ is derived

$$\boldsymbol{v}_{dq0}(n) = -\mathbf{R}_{dq0}\boldsymbol{i}_{dq0}(n) + \boldsymbol{v}^{\mathrm{hist}}_{dq0,\mathrm{eq}} \tag{34}$$

where

$$\mathbf{R}_{dq0} = \mathbf{R}_{ss} - \mathbf{R}_{sr}\mathbf{R}_{rr}^{-1}\mathbf{R}_{rs} \tag{35}$$

$$\boldsymbol{v}^{\mathrm{hist}}_{dq0,\mathrm{eq}} = -\mathbf{R}_{sr}\mathbf{R}_{rr}^{-1}\{-\boldsymbol{v}_r(n) + \boldsymbol{v}^{\mathrm{hist}}_r\} + \boldsymbol{v}^{\mathrm{hist}}_{dq0}. \tag{36}$$

The equivalent voltage source $\boldsymbol{v}_{abc,\mathrm{eq}}(n)$ and resistance $\mathbf{R}_{abc,\mathrm{eq}}(n)$ can be obtained by transforming (34) into abc frame using the Park's transformation matrix $\mathbf{P}_n$:

$$\mathbf{R}_{abc,\mathrm{eq}}(n) = \mathbf{P}_n^{-1}\mathbf{R}_{dq0}\mathbf{P}_n, \quad \boldsymbol{v}_{abc,\mathrm{eq}}(n) = \mathbf{P}_n^{-1}\boldsymbol{v}^{\mathrm{hist}}_{dq0,\mathrm{eq}}. \tag{37}$$

The change of ω is handled by the mechanical equation, and since ω at time t_n is unknown while solving the machine equations, it is predicted first and then updated iteratively by solving the network equations until convergence.

The AC4A type exciter model in PSCAD/EMTDC [5] is adopted to make the machine work stable. As can be seen in the diagram, it also involves the convolution operation when passing the transfer function that has the same format with transmission lines. Thus, it has the same step-by-step calculation flow of convolution as described in the ULM model.

IV. Real-Time Emulator Implementation

To test and verify the proposed ATS transmission line and machine models on a large power system, an IEEE 39-bus system composed of 34 transmission lines and 10 generators was selected as the case study.

A. Circuit Topology

As shown in Fig. 5(a), the power system consists of 34 transmission lines, ten generators, 12 transformers, and 19 loads. Since the power transformer and RLC loads are not the main focus of this article, the lumped parameter transformer model based on admittance matrix representation [23] without saturation utilized. When the time-step changes, the equivalent resistance of L and C will change, which only causes the change of the equivalent admittance matrix of the system.

B. Hardware Implementation

The Virtex UltraScale+ FPGA VCU118 board [24] used in this article contains both highly programmable UltraScale XCVU9P device and rich external resources. Considering the heavy computation task within each time-step and the large system scale, the multiboard solution is adopted, in which two VCU118 boards were interfaced through SFP transceivers, and each board only models a part of the system.

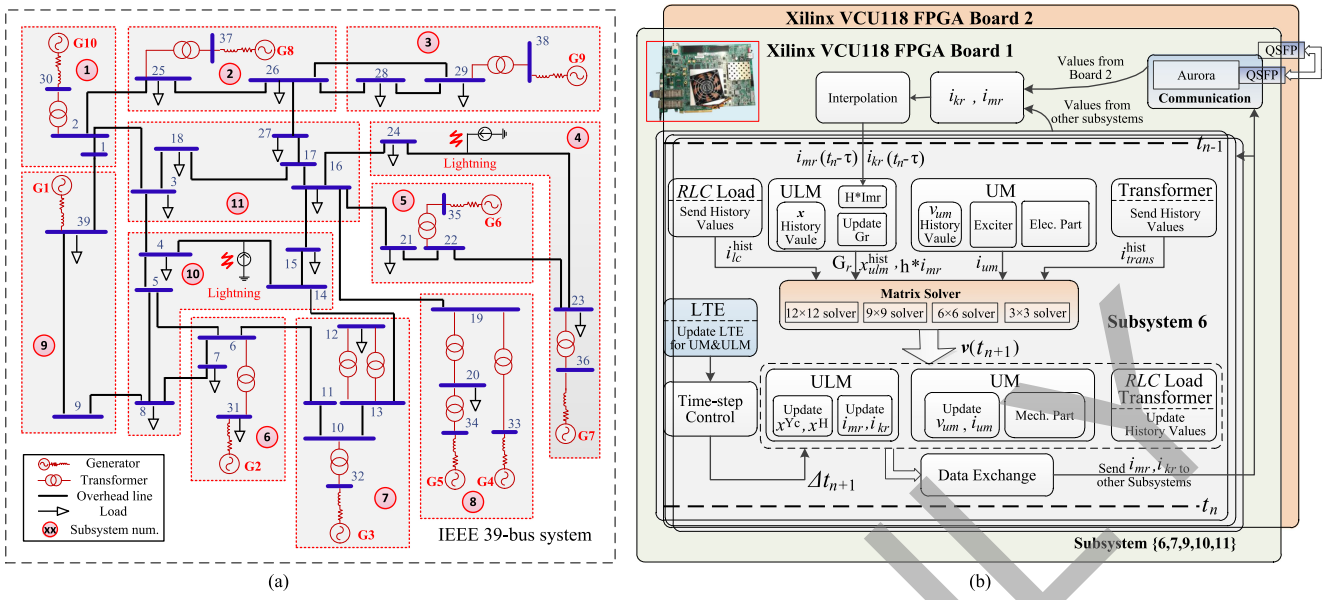

Fig. 5. Test system and the hardware emulation on two interfaced FPGA boards.

Subsystem Allocation: As shown in Fig. 5(a), the power system is divided into 11 subsystems taking advantage of the distributed transmission lines, and the connected subsystems exchange data (i_{mr} and i_{kr}) after calculation of each time-step. Since almost every generator is connected with a transformer, it is convenient to implement if every generator–transformer pair is allocated to an individual subsystem, as marked as subsystem S_1–S_6 in Fig. 5(a). In each subsystem, the transmission lines can again divide the subsystem into subsubsystems, which effectively reduces the size of admittance matrix to be solved. For example, the maximum matrix size of S_9–S_{11} is 3×3, S_1–S_6 is 6×6. S_7 and S_8 have the largest matrix to solve due the coupled transformers, which are 9×9 and 12×12, respectively. Since the transients happen in subsystem S_{10} and S_4, to reduce the latency of data exchange between connected subsystems, the subsystems (S_6, S_7, S_9, S_{10}, S_{11}) that are connected with S_{10} are all allocated at the same FPGA board, and the other six subsystems are allocated to another FPGA board. The board-to-board communication is handled by the lightweight communication protocol Aurora [25], which is supported by different type of transceivers such as GTX, GTY, and GTH, was used. The two boards are interfaced via 2 Aurora lanes, with 32b floating point data transferred in each lane.

Adaptive Time-Step Control: In this article, four time-step sizes are applied: 5, 10, 20, and 40 μs. Considering the matrix to be solved in different subsystems may be different and some subsystems contain generators that will occupy more time-space to compute, the time-step set of different subsystems are different. After the minimum computing latency of each subsystem is obtained through hardware implementation (the results are shown in Section C), the proper time-step set can be determined: subsystem S_1–S_6 has the same time-step set $\{10, 20, 40\ \mu s\}$, subsystem S_7–S_8 has the same time-step set $\{20, 40\ \mu s\}$, and subsystem S_9–S_{11} has the same time-step set $\{5, 10, 20\ \mu s\}$.

TABLE I
DEMONSTRATION OF FTRT

Mode	Subsystem	Δt	t_p	Subsystem	Δt	t_p
RT	S_{10}	$5\mu s$ $10\mu s$	$5\mu s$ $10\mu s$	S_1	$10\mu s$ $10\mu s$	$10\mu s$ $10\mu s$
FTRT2	S_{10}	$10\mu s$ $20\mu s$	$5\mu s$ $10\mu s$	S_1	$20\mu s$ $40\mu s$	$10\mu s$ $20\mu s$
FTRT4	S_{10}	$20\mu s$	$5\mu s$	S_1	$40\mu s$	$10\mu s$

The time-step increase or decrease is determined by the LTE of the previous step and the threshold, wherein the threshold of various subsystems are also different. For the subsystems where transients happen, the LTE threshold is relatively smaller compared with that of the other subsystems.

Faster-Than-Real-Time (FTRT): Although the system with FTS can also be implemented in real time, the main advantage of variable time-step is to accelerate the simulation progress without loss of accuracy. Thus the proposed ATS simulation could be even faster-than-real-time, which means, the actual processing time of each step is smaller than the time-step applied for the simulation. FTRT can be achieved by proper coordination between different subsystems. First, the maximum processing latency of a subsystem limits the minimum time-step of the subsystem that implies that the large time-step is actually achieved by adding a time space between two steps. If the time space size can be narrowed synergistically, the simulation time will be reduced when the time-step changes to be larger than the minimum time-step. Second, the narrowed time space should be consistent among different subsystems, because the time-step of various subsystems may be different and it will easily cause inconsistency if the actual latency is not reduced proportionally.

Take subsystems S1 and S10 as an example, their time-step Δt and actual processing time t_p is illustrated in Table I. The

TABLE II
PROCESSING LATENCY OF DIFFERENT SUBSYSTEMS

Subsystem/Element	Latency	Subsystem/Element	Latency
Subsystem 1∼6	9.7μs	Subsystem 7	14.6μs
Subsystem 8	19.2μs	Subsystem 9	4.8μs
Subsystem 10∼11	3.3μs	Trans. Line	1.05μs

TABLE III
HARDWARE RESOURCE UTILIZATION OF THE CASE STUDY

Resource	VCU118-Board1	VCU118-Board2
Subsystems	S_6, S_7, S_9, S_{10}, S_{11}	S_1, S_2, S_3, S_4, S_5, S_8
LUT	767,174 (64.9%)	819,148 (69.3%)
FF	927,012 (39.2%)	1,014,011 (42.8%)
DSP	6,448 (94.3%)	6,714 (98.1%)
BRAM	570 (26.4%)	624 (28.9%)

minimum time-step of S1 and S10 is near 10 μs and 5 μs, respectively, thus the time-step of 10 and 5 μs cannot be reduced. As shown in the second row, if S1 runs at 10 μs, the latency of S10 with time-step size of 10 μs also could not be reduced because the processing time of S1 cannot be smaller than 10 μs. This indicates that no matter which subsystem was running at the minimum time-step (typically is under transient condition), the latency of other subsystems cannot be reduced. Under normal steady-state conditions the time-step of all subsystems is usually changed to larger values, in this case, the actual latency can be reduced to make the simulation faster, as shown in the last three rows in Table I. Note that FTRT2 means two times faster, and FTRT4 means four times faster.

C. Latency and Hardware Resource Utilization

The latency of different subsystems on hardware are recorded in Table II, which indicates the minimum time-step that can be applied for different subsystems. For example, subsystem S_8 consumes the most latency because it involves the iteration for UM and has the largest matrix (12×12) to solve. The hardware resource consumption on the two VCU118 boards is presented in Table III.

V. RESULTS AND VERIFICATION

The test case described in Section IV was emulated on the two FPGA boards and the results are compared with PSCAD/EMTDC to show the effectiveness of the proposed ATS models. Note that PSCAD/EMTDC is only a representative of fixed time-stepping EMT simulation tools, and it does not matter if other software are used for comparison because the ULM and UM model with FTSs are both commonly used models. The clock frequency of FPGA boards is set at 100 MHz.

A. Verification of the ULM Model

Before the ULM model is integrated into the IEEE 39-bus system, it is necessary to verify the stability of the proposed process-reversed method. Note that the UM model in ATS is stable because the state variable remains the same when the time-step changes. To solely validate the proposed ULM model, the subsystem S_9 in Fig. 5(a) with ideal voltage source is simulated while keeping the load and connection with other subsystems as open circuit. At time 0.005 s, the time-step changes from 10 to 20 μs; and at time 0.035 s, the time-step changes from 20 to 50 μs.

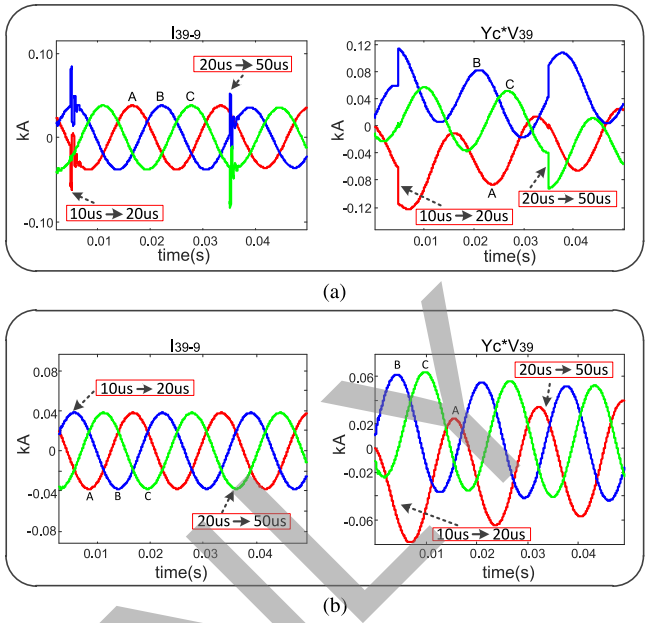

Fig. 6. Waveforms under time-step change operation. (a) Traditional ULM model. (b) Proposed process-reversed ULM model.

The results of i_{39-9} (from Bus39 to Bus9) and $\mathbf{Y}_c * v_{39}$ using the traditional model are shown in Fig. 6(a), when the time-step changes, there will have a large oscillation. Since the actual state variable changes when the time-step changes, the initial value of the new state variable will be incorrect, which causes an abrupt change of the convolution results. However, when using the proposed process-reversed model, it can be observed that the convolution results will remain continuous and stable, which results in a stable current i_{39-9} when the time-step changes.

B. Real-Time Simulation Results

To simulate the dynamic behavior of the system, the lightning surge at phase C of transmission line L_{4-14} (between bus 4 and bus 14) and L_{23-24} is chosen as the transient test. The results are evaluated by the proposed emulator and PSCAD/EMTDC that used a FTS of 10 μs while the proposed emulator used adaptive time-steps described in Section IV. The standard $10/350\,\mu$s lightning surge current [26] is applied in this article, given as

$$I_{\mathrm{LS}}(t) = CI_m(t/\tau_1)^k e^{\frac{-t}{\tau_2}} / \left[1 + (t/\tau_1)^k\right] \tag{38}$$

where the coefficient $C = 1.075$, $k = 10$; the time constant $\tau_1 = 19\,\mu$s, $\tau_2 = 485\,\mu$s; the maximum value of the surge current $I_m = 3$ kA. The lightning surge current at L_{4-14} and L_{23-24} is applied at exactly 2 and 2.5 s of the simulation to demonstrate the transient behavior of ULM and UM, respectively.

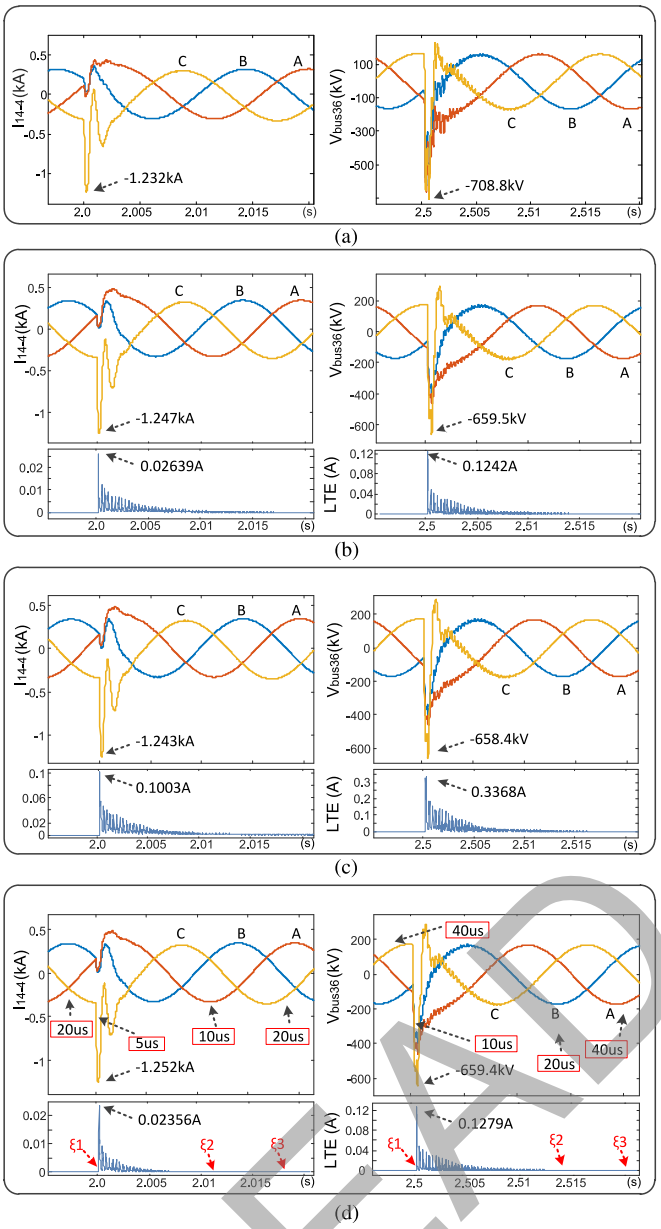

Fig. 7. Lightning transient results of i_{14-4} and $v_{\text{bus}36}$. (a) PSCAD results with 10 μs FTS. (b), (c) FPGA-based emulator with 10 and 20 μs time-steps. (d) FPGA-based emulator with ATS.

TABLE IV
MINIMUM TIME-STEP SIZE AND MAXIMUM LTE OF ULM AND UM UNDER LIGHTNING TRANSIENT

Element	FTS-10μs	FTS-20μs	ATS
ULM	$10\mu s, 0.02639$A	$20\mu s, 0.1003A$	$5\mu s, 0.02356$A
UM	$10\mu s, 0.1242$A	$20\mu s, 0.3368$A	$10\mu s, 0.1279$A

First, the simulation is executed in real time and compared with PSCAD and the hardware emulator with FTS, and the results are recorded in Fig. 7 and Table IV. The FTS emulator applies the same time-step for the entire system. Since the maximum processing latency of the decomposed subsystems is near 20 μs, FTS-20 μs is actually the FTS emulator with minimum time-step size that can be achieved in real time. But through the proposed subsystem-based ATS scheme, the entire system can be simulated in real time with smaller time-step sizes by applying different variable time-steps for different subsystems. From Fig. 7(a) and (b) with the same time-step size it can be observed that the peak values of the machine terminal voltage under transients are -708.8 and -659.5 kV, respectively, which indicates that the UM model implemented in this article is more stable than PSCAD.

In Fig. 7(b) and (c) and Table IV, the emulator with 10 μs time-step size produces a smaller LTE, and the peak value of LTEs of ULM and UM reduces 63.1% and 73.7%, respectively, compared with that using a 20 μs time-step. That means reducing the time-step size will generate a more accurate result. The results using ATS are shown in Fig. 7(d), from which we can see the large time-step is applied under the normal operation, and when the transient happens, the time-step is reduced automatically according to the LTE. For example, the time-step is 20 μs for L_{14-4} before the lightning, and when the transient happens, the LTE directly rises to an extremely large value that exceed the max threshold ξ_1 immediately, then the time-step reduces to the minimum one (5 μs) directly. When the LTE is below ξ_2, the time-step increases into a larger one (10 μs), and as the LTE is reduced below the minimum threshold ξ_3, the time-step regains to the maximum one (20 μs). Since the time-step size of ULM reduces to 5 μs under transients, the maximum LTE reduces 76.5% compared with that of FTS-20 μs. The UM has the same process although the time-step set is not the same since L_{14-4} and L_{23-24} belongs to the different subsystems.

The UM model cannot be executed in a time-step less than 10 μs, thus the minimum time-step size of UM is 10 μs, resulting in a LTE 62.0% smaller than that of FTS-20 μs. The LTE of ATS is a little different with FTS-10 μs because the time-step sizes in ATS also vary between subsystems while FTS-10 μs applies the same time-step for the whole system.

Second, to show the acceleration of the ATS simulation, the transient simulation is carried in FTRT2 mode (shown in Table I) through elaborate configurations and compared with the results of real-time simulation. Fig. 8 demonstrates the Bus 36 voltage of subsystem S_4, it can be observed the two versions have the same numerical results because the time-steps and parameters applied are the same. But due to the different actual processing time of each step, the output rate of the results are different. The FTRT version can produce data at a faster rate than the real-time simulation under normal operations, although under lightning transient they have the same output rate. In this article, only the simulation with 40 μs is accelerated by two times, because as described in Section IV, the minimum time-step cannot be accelerated. Since the duration of simulation with 20 μs is quite small, to reduce the complexity of simulation time control logic, it is not necessary to accelerate it. Besides, the maximum time-step is only four times of the minimum time-step in this article, it can be concluded that if the maximum time-step is larger, the output rate will be even faster than real time.

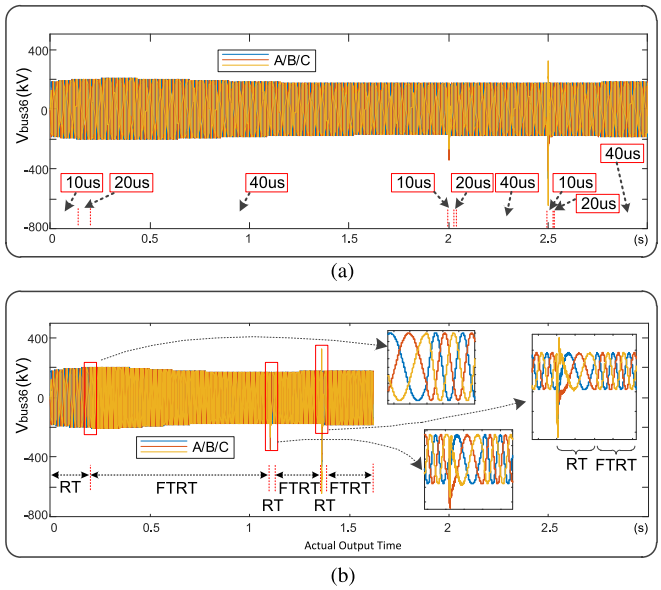

Fig. 8. Demonstration of FTRT results. (a) Real-time results in ATS; (b) Results of FTRT2 mode in ATS.

VI. Conclusion

In this article, the ATS universal transmission line model and UM model were proposed for the accurate EMT simulation of power systems in real time and faster-than-real-time mode. In the proposed ULM model, through a novel process-reversal of the traditional model, the stability was significantly improved during the time-step change operation. By using LTE as the time-step change criteria, the time-step can be adjusted properly when the transient happens. The hardware emulator for large-scale power systems was presented, in which the system was divided into small subsystems and each subsystem maintains its own time-step set and the LTE threshold. By elaborate coordination between subsystems, the faster-than-real-time mode can be achieved. The IEEE 39-bus power system was emulated in both real time and the FTRT mode. The hardware resource cost and processing delay of different subsystems were evaluated, which showed the practicality of ATS for transient simulation. The real-time emulation results were captured and compared with PSCAD/EMTDC, which demonstrated the effectiveness of the proposed models. The proposed ATS-based ULM and UM model and the hardware emulation architecture can be used for the FTRT EMT simulation of large power systems. In the future work, the ATS models for the other power equipment such as the detailed transformer model will be studied, and more phenomena such as hysteresis and nonlinear saturation could also be taken into consideration for the ATS EMT simulation. ATS power electronic apparatus models can also be integrated with the proposed ATS-based ULM and UM models for a comprehensive ac–dc grid real-time simulation.

Appendix

Parameters of the test system [27]: Base values: 100 MVA, 230 kV, 60 Hz; Generator and loads: given in [27]; transformers: 230 kV/230 kV, leakage inductance 0.2 p.u., copper loss 0.004 p.u.; transmission lines: the length of lines in the IEEE 39-bus system are given in [27].

References

[1] G. G. Parma and V. Dinavahi, "Real-time digital hardware simulation of power electronics and drives," *IEEE Trans. Power Del.*, vol. 22, no. 2, pp. 1235–1246, Apr. 2007.
[2] B. Lu, X. Wu, H. Figueroa, and A. Monti, "A low-cost real-time hardware-in-the-loop testing approach of power electronics controls," *IEEE Trans. Ind. Electron.*, vol. 54, no. 2, pp. 919–931, Apr. 2007.
[3] M. O. Faruque and V. Dinavahi, "Hardware-in-the-loop simulation of power electronic systems using adaptive discretization," *IEEE Trans. Ind. Electron.*, vol. 57, no. 4, pp. 1146–1158, Apr. 2010.
[4] M. S. Vekić, S. U. Grabić, D. P. Majstorović, I. L. Čaelanović, N. L. Čelanović, and V. A. Katić, "Ultralow latency HIL platform for rapid development of complex power electronics systems," *IEEE Trans. Power Electron.*, vol. 27, no. 11, pp. 4436–4444, Nov. 2012.
[5] *EMTDC User's Guide: A Comprehensive Resource for EMTDC,*Version 4.7, Manitoba HVDC Research Centre, Winnipeg, MB, Canada, 2010.
[6] J. J. Sanchez-Gasca, R. D'Aquila, J. J. Paserba, W. W. Price, D. B. Klapper, and I.-. Hu, "Extended-term dynamic simulation using variable time step integration," *IEEE Comput. Appl. Power*, vol. 6, no. 4, pp. 23–28, Oct. 1993.
[7] S. Hui, K. Fung, M. Zhang, and C. Christopoulos, "Variable time step technique for transmission line modeling," *IEE Proc. A - Sci., Meas. Technol.*, vol. 140, no. 4, pp. 299–302, Jul. 1993.
[8] J. J. Sanchez-Gasca, R. D'Aquila, W. W. Price, and J. J. Paserba, "Variable time step, implicit integration for extended-term power system dynamic simulation," in *Proc. IEEE Power Ind. Comput. Appl. Conf.*, Salt Lake City, CA, USA, May 1995, pp. 183–189.
[9] S. Henschel, A. I. Ibrahim, and H. W. Dommel, "Transmission line model for variable step size simulation algorithms," *Int. J. Elect. Power Energy Syst.*, vol. 21, no. 3, pp. 191–198, Mar. 1999.
[10] A. Ramirez and R. Iravani, "Frequency-domain simulation of electromagnetic transients using variable sampling time-step," *IEEE Trans. Power Del.*, vol. 30, no. 6, pp. 2602–2604, Dec. 2015.
[11] F. Camara, A. C. S. Lima, and K. Strunz, "Full-frequency dependent models for variable time-step simulations," CIGRE Session Papers Proc. no. C4-302, pp. 1–11, 2018.
[12] Z. Shen and V. Dinavahi, "Dynamic variable time-stepping schemes for real-time FPGA-based nonlinear electromagnetic transient emulation," *IEEE Trans. Ind. Electron.*, vol. 64, no. 5, pp. 4006–4016, Jan. 2017.
[13] N. Lin and V. Dinavahi, "Variable time-stepping modular multilevel converter model for fast and parallel transient simulation of multiterminal DC grid," *IEEE Trans. Ind. Electron.*, vol. 66, no. 9, pp. 6661–6670, Sep. 2019.
[14] H. W. Dommel, *EMTP Theory Book.* Portland, OR, USA: Bonneville Power Administration, 1984.
[15] A. Morched, B. Gustavsen, and M. Tartibi, "A universal model for accurate calculation of electromagnetic transients on overhead lines and underground cables," *IEEE Trans. Power Del.*, vol. 14, no. 3, pp. 1032–1038, Jul. 1999.
[16] H. K. Lauw and W. Scott Meyer, "Universal machine modeling for the representation of rotating electric machinery in an electromagnetic transients program," *IEEE Trans. Power Appl. Syst.*, vol. 101, no. 6, pp. 1342–1351, Jun. 1982.
[17] C. Deml and P. Turkes, "Fast simulation technique for power electronic circuits with widely different time constants," *IEEE Trans. Ind. Appl.*, vol. 35, no. 3, pp. 657–662, May 1999.
[18] F. N. Najm, *Circuit Simulation.* Hoboken, NJ, USA: Wiley, pp. 241–252, 2010.
[19] B. Gustavsen and A. Semlyen, "Simulation of transmission line transients using vector fitting and modal decomposition," *IEEE Trans. Power Del.*, vol. 13, no. 2, pp. 605–614, Apr. 1998.
[20] B. Gustavsen, G. Irwin, R. Mangelrod, D. Brandt, and K. Kent, "Transmission line models for the simulation of interaction phenomena between parallel AC and DC overhead lines," in *Proc. Int. Conf. Power Syst. Transients*, Budapest, Hungary, Jun. 1999, pp. 61–68.
[21] Y. Chen and V. Dinavahi, "Digital hardware emulation of universal machine and universal line models for real-time electromagnetic transient simulation," *IEEE Trans. Ind. Electron.*, vol. 59, no. 2, pp. 1300–1309, Feb. 2012.

[22] L. Wang and J. Jatskevich, "A voltage-behind-reactance synchronous machine model for the EMTP-type solution," *IEEE Trans. Power Syst.*, vol. 21, no. 4, pp. 1539–1549, Nov. 2006.
[23] J. Liu and V. Dinavahi, "A real-time nonlinear hysteretic power transformer transient model on FPGA," *IEEE Trans. Ind. Electron.*, vol. 61, no. 7, pp. 3587–3597, Jul. 2014.
[24] *VCU118 Evaluation Board User Guide (UG1224)*, Xilinx Inc., San Jose, CA, USA, Oct. 2018.
[25] *Aurora 64B/66B LogiCORE IP Product Guide, PG074 (V11.2)*, Xilinx Inc., San Jose, CA, USA, Apr. 2018.
[26] R. B. Standler, '*Protection Against Lightning Electromagnetic Impulse - Part I : General Principles*, IEC Standard 1312-I, Feb. 1995.
[27] *PSCAD IEEE 39 Bus System*, Revision 1, Manitoba HVDC Research Centre, Winnipeg, MB, Canada, 2010.

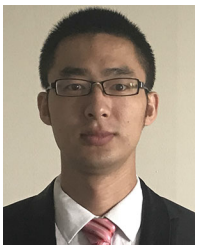

Tong Duan (S'18) received the B.Eng. degree in electrical engineering from Tsinghua University, Beijing, China, in 2013. He is currently working toward the Ph.D. degree in electrical and computer engineering, University of Alberta, Edmonton, AB, Canada.

His research interests include real-time simulation of power systems, power electronics, and field-programmable gate arrays.

Venkata Dinavahi (S'94–M'00–SM'08) received the B.Eng. degree from the Visveswaraya National Institute of Technology, Nagpur, India, in 1993, and the M.Tech. degree from the Indian Institute of Technology (IIT) Kanpur, India, in 1996, both in electrical engineering, and the Ph.D. degree in electrical and computer engineering from the University of Toronto, ON, Canada, in 2000.

He is currently a Professor with the Department of Electrical and Computer Engineering, University of Alberta, Edmonton, AB, Canada. His research interests include real-time simulation of power systems and power electronic systems, electromagnetic transients, device-level modeling, large-scale systems, and parallel and distributed computing.